J. Appl. Phys. Vol.96, No.7 (2004), pp.3839-3844
HTML ABSTRACT + LINKS 0021-8979/2004/96(7)3839/6/ copyright 2004 American Institute of Physics
JOURNAL OF APPLIED PHYSICS VOLUME 96, NUMBER 7 1 OCTOBER 2004

High frequency response of *p-i-n* photodiodes analyzed by an analytical model in Fourier space

K. Konno,[a] O. Matsushima, D. Navarro, and M. Miura-Mattausch
Graduate School of Advanced Sciences of Matter, Hiroshima University, Higashi-Hiroshima 739-8530, Japan

(Received 13 April 2004; accepted 8 July 2004)

A formulation of carrier transport in vertical *p-i-n* photodiodes is presented in Fourier space, taking into account diffusion effects of carriers outside the intrinsic region. High frequency response of photodiodes is investigated using the model. Calculated results show that diffusion limits the cutoff frequency characteristics of photodiodes with short intrinsic region length. Photocurrent calculations via the spectral method are in excellent agreement with two-dimensional device simulator results. The model can be utilized in circuit simulation because of its reduced computational runtime. © *2004 American Institute of Physics*. [DOI: 10.1063/1.1787616]

I. INTRODUCTION

In order to design optoelectronic integrated circuits (OEIC), accurate physics-based models describing the characteristics of optoelectronic devices are necessary. One such device is the *p-i-n* photodiode, which has been generally investigated by solving the basic device equations using two approaches: full numerical approach[1–4] and analytical approach.[5–9] For models employed in circuit simulation, the latter is more appropriate because the computational time is considerably reduced, and thus adopted here. We particularly focus on the vertical *p-i-n* photodiode, typically used as photodetector in OEIC.

The high frequency response of the photodiode is mainly limited by three factors.[8,9]

(1) The drift transit time τ_{dr} for carriers to cross intrinsic (i) region.
(2) The time τ_{RC} arising from junction capacitance C and load resistance R.
(3) The diffusion time τ_{diff} of carriers generated in n^+ and/or p^+ region.

The first factor is discussed precisely in previous works[5–9] by considering the i region of the photodiode. In this region, the carriers move along the direction of the electric field E applied. Thus the time τ_{dr} to cross the i region of length L is given by $\tau_{dr}=L/\mu E$, where μ is the mobility of carriers and E is the magnitude of the electric field. Therefore the cutoff frequency f_T is inversely proportional to L, i.e., $f_{T,dr}\sim 1/\tau_{dr} \propto 1/L$. This describes a fact that long L is not suitable for high frequency operation.

The second factor, RC-constant effect, has been taken into account in Refs. 8 and 9. A reverse-biased *p-i-n* photodiode is treated as a capacitor, with the capacitance described by $C\propto 1/L$. Thus τ_{RC} is also proportional to $1/L$, which gives $f_{T,RC}\sim 1/RC\propto L/R$. Therefore, the RC-constant effect becomes evident at small L. It is worthwhile to note that the cutoff frequency increases as the load resistance R decreases, and vice versa. However, it is expected that diffusion (the third limiting factor) becomes dominant and determines the cutoff frequency as R decreases. The combination of the three limiting factors is shown in Fig. 1. The high frequency response at small L is determined either by RC effect or diffusion depending on the value of R. Physically, as L approaches 0, *p-i-n* becomes similar to a *pn* photodiode. In such case, most of the carriers are created in the low electric field region and diffuse towards the junction. However, diffusion is often neglected in analytical formulations and its effect on high frequency response is not investigated yet.

In this paper, we present a consistent formulation for the current characteristics of the vertical *p-i-n* photodiode by taking into account the carrier diffusion generated in the n or p region. Furthermore, we elucidate the role of each limiting factor on the high frequency response of the photodiode. A simulation scheme based on the spectral method[10] is also described using analytical solution in Fourier space. In spite of significant reduction in calculation time, the accuracy of

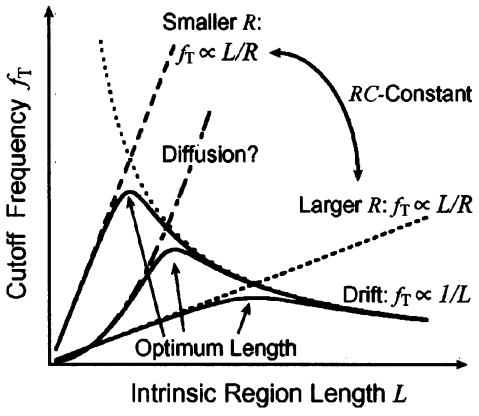

FIG. 1. Schematic illustration of the limiting factors to cutoff frequency f_T as a function of intrinsic region length L. The dotted curve denotes the limiting factor due to drift, which is proportional to $1/L$. The two dashed lines denote the RC-constant effect, which is proportional to L/R. Expected effect of diffusion is also depicted. The combination of these limiting factors determines the optimum length of intrinsic region to obtain high frequency response.

[a]Electronic mail: kohkichi@hiroshima-u.ac.jp

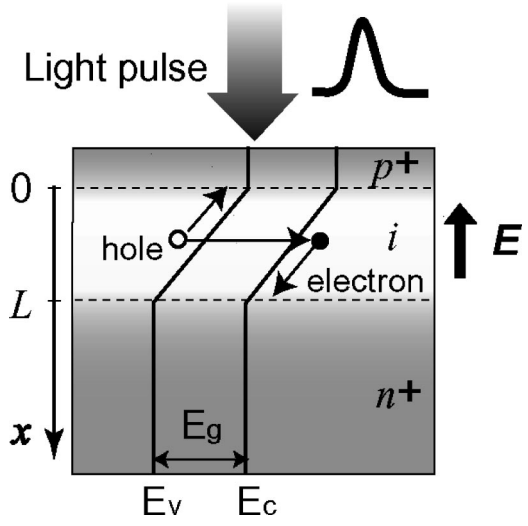

FIG. 2. Structure of the vertical *p-i-n* photodiode. Light pulse is applied on the *p* surface and the generated carriers cross the junction.

our calculation results are comparable to those of a conventional two-dimensional numerical device simulator.

The organization of this paper is as follows. In Sec. II, we discuss the structure of the vertical *p-i-n* photodiode and the basic equations governing carrier transport. In Sec. III, the stationary approximation is briefly reviewed. Secion IV is devoted to the derivation of nonstationary description of carrier transport. Using the Fourier expansion, we investigate the high frequency photoresponse of the photodiode. Finally we give a summary in Sec. V.

II. VERTICAL *P-I-N* PHOTODIODE STRUCTURE AND DEVICE EQUATIONS

The vertical *p-i-n* photodiode device structure is shown in Fig. 2. Light pulse is applied on the *p* surface. Generated carriers cross the junction and flow as photocurrent. In order to derive equations for the current, we adopt the following assumptions.

(1) Homogeneity in all device parameters, as well as the intensity of the light radiation normal to the x axis in Fig. 2.
(2) Constant electric field E_0 in the i region.
(3) Negligible potential drop in the p^+ and n^+ region.
(4) Shallow p^+ region with respect to light penetration depth.
(5) No change of electric field due to the incident light pulse.

From the first assumption, we can treat the carrier dynamics only in one dimension, along the x direction. To minimize diffusing carriers generated in the p^+ region, the fourth assumption is introduced. Therefore, we neglect the $p^+(x<0)$ region hereafter. The last one implies that we can approximate the electric field $E(x)$ as

$$\frac{dE(x)}{dx} \simeq \frac{q}{\varepsilon}\left[N_D^+(x) - N_A^-(x)\right], \tag{1}$$

where q, ε, N_D^+, and N_A^- are the elementary charge, the permittivity, and the densities of ionized donors and acceptors, respectively (see, e.g., Ref.11 for higher intensity illumination). This assumption is justified by the fact that the ordinary operating condition of photodiodes is in the linear region in which the incident light intensity is below the level from which the output pulse shape is distorted due to screening effect. The solution of this equation is approximated as

$$E(x) \simeq \begin{cases} E_0 & (0 \leqslant x \leqslant L) \\ 0 & (x > L) \end{cases}. \tag{2}$$

The equations governing carrier transport are given by

$$\frac{\partial n(x,t)}{\partial t} - \frac{1}{q}\frac{\partial J_n(x,t)}{\partial x} = G_n(x,t) - R_n(x,t), \tag{3}$$

$$\frac{\partial p(x,t)}{\partial t} + \frac{1}{q}\frac{\partial J_p(x,t)}{\partial x} = G_p(x,t) - R_p(x,t), \tag{4}$$

where n and p are the electron and hole density, J_n and J_p are the electron and hole current density, G is the carrier generation rate, and R is the carrier recombination rate. We now adopt the drift-diffusion approximation. For $0 \leqslant x \leqslant L$

$$J_n(x,t) \simeq q\mu_n n(x,t)E(x), \tag{5}$$

$$J_p(x,t) \simeq q\mu_p p(x,t)E(x), \tag{6}$$

and for $x > L$

$$J_p(x,t) \simeq -kT\mu_p \frac{\partial p(x,t)}{\partial x}, \tag{7}$$

where $\mu_{n,p}$ is the mobility. Since high reverse bias is normally applied to obtain high speed operation, the drift component overwhelms the diffusion component in the intrinsic region, and thus the latter component can be neglected. On the other hand, in the region of $x > L$, the electric field due to the high reverse bias vanishes and thus diffusion comes into play. The generation rate G and recombination rate R are given by

$$G_{n,p}(x,t) = \alpha\phi(t)e^{-\alpha x}, \tag{8}$$

$$R_p(x,t) = \begin{cases} 0 & (0 \leqslant x \leqslant L) \\ \dfrac{p(x) - p_0}{\tau_p} & (x > L) \end{cases}, \tag{9}$$

where α, ϕ, p_0, and τ_p are the absorption coefficient of the incident light, the photon flux, the hole density of n^+ substrate in equilibrium, and the life time of holes, respectively. Here, we adopt the relaxation time approximation as the recombination rate. In the intrinsic region, carriers quickly evacuate to the n^+ or p^+ region due to the high electric field, and thus recombination can be neglected. Moreover, the dwell time τ_d that carriers are in the i region can be roughly estimated as $\tau_d = L/\mu E_0 \sim 2 \times 10^{-11}$ s$(L/1\ \mu\text{m}) \times (500\ \text{cm}^2\ \text{V}^{-1}\ \text{s}^{-1}/\mu)(10^4\ \text{V cm}^{-1}/E_0)$, which is very much shorter than carrier lifetime. Thus, our approximation is

valid. The assumptions which we adopted in this section are reasonable even in realistic cases (see also Ref. 5).

III. STATIONARY DESCRIPTION OF THE PHOTODIODE CHARACTERISTICS

Before discussing the nonstationary features of the photodiode, the stationary solution, which is derived by setting the time derivatives to zero, is reviewed (see the text book of S. M. Sze[12]). The solution is valid in describing the photodiode characteristics under constant to low frequency variation of incident light.

In the i region ($0 \leqslant x \leqslant L$), we derive the differential equations

$$\frac{dJ_n(x)}{dx} = -q\alpha\phi e^{-\alpha x}, \tag{10}$$

$$\frac{dJ_p(x)}{dx} = q\alpha\phi e^{-\alpha x}. \tag{11}$$

The solution satisfying the boundary conditions

$$J_n(0) = 0, \quad J_p(L) = 0 \tag{12}$$

is given by

$$J_n(x) = q\phi(e^{-\alpha x} - 1), \tag{13}$$

$$J_p(x) = q\phi(e^{-\alpha L} - e^{-\alpha x}). \tag{14}$$

Therefore, the current due to the drift becomes

$$J_{\mathrm{dr}} = J_n + J_p = -q\phi(1 - e^{-\alpha L}). \tag{15}$$

In the n^+ region ($x > L$), we derive the differential equation

$$D_p\frac{d^2p(x)}{dx^2} - \frac{p(x) - p_0}{\tau_p} = -\alpha\phi\, e^{-\alpha x}, \tag{16}$$

where $D_p = \mu_p kT/q$. Under the boundary conditions

$$p(\infty) = p_0, \quad p(L) = 0, \tag{17}$$

we can obtain the solution as

$$p(x) = p_0 - \left(p_{n0} + \frac{\alpha L_p^2}{1 - \alpha^2 L_p^2}\frac{\phi}{D_p}e^{-\alpha L}\right)e^{-(x-L)/L_p} + \frac{\alpha L_p^2}{1 - \alpha^2 L_p^2}\frac{\phi}{D_p}e^{-\alpha x}, \tag{18}$$

where $L_p = \sqrt{D_p\tau_p}$. Therefore, the current density at $x = L$ is written as

$$\begin{aligned} J_{\mathrm{diff}}(L) &= -qD_p\left(\frac{dp(x)}{dx}\right)_{x=L} \\ &= -qp_0\frac{D_p}{L_p} - q\phi\frac{\alpha L_p}{1 + \alpha L_p}e^{-\alpha L} \\ &\simeq -q\phi\frac{\alpha L_p}{1 + \alpha L_p}e^{-\alpha L}. \end{aligned} \tag{19}$$

The total current density is the sum of the drift and diffusion components

$$J_{\mathrm{total}}(L) = J_{\mathrm{dr}}(L) + J_{\mathrm{diff}}(L) = -q\phi\left(1 - \frac{e^{-\alpha L}}{1 + \alpha L_p}\right). \tag{20}$$

The response of the photodiode to a low frequency incident light variation can be described by the time variation of the photon flux ϕ. In the following section, based on the above formulation, we present nonstationary description taking into account time derivative terms.

IV. FULL NONSTATIONARY DESCRIPTION OF THE PHOTODIODE CHARACTERISTICS

Here, we present a description for the nonstationary case under high frequency operation of photodiodes. We adopt the Fourier expansion method, which eliminates the variable t and transforms the partial differential equations to a set of solvable second-order ordinary differential equations.

A. Formulation using Fourier expansion

First, we expand $n(x,t), p(x,t), \phi(t), J_n(x,t)$, and $J_p(x,t)$ as

$$n(x,t) = \sum_{\omega_i} n_{\omega_i}(x)e^{-i\omega_i t}, \tag{21}$$

$$p(x,t) = \sum_{\omega_i} p_{\omega_i}(x)e^{-i\omega_i t}, \tag{22}$$

$$\phi(t) = \sum_{\omega_i} \phi_{\omega_i}e^{-i\omega_i t}, \tag{23}$$

$$J_n(x,t) = \sum_{\omega_i} J_{n,\omega_i}(x)e^{-i\omega_i t}, \tag{24}$$

$$J_p(x,t) = \sum_{\omega_i} J_{p,\omega_i}(x)e^{-i\omega_i t}, \tag{25}$$

where ω_i is the modulation frequency.

In the i region ($0 \leqslant x \leqslant L$), from Eqs. (3)–(6), we derive the differential equations

$$\frac{dn_{\omega_i}(x)}{dx} + \frac{i\omega_i}{\mu_n E_0}n_{\omega_i}(x) = -\frac{\alpha\phi_{\omega_i}}{\mu_n E_0}e^{-\alpha x}, \tag{26}$$

$$\frac{dp_{\omega_i}(x)}{dx} - \frac{i\omega_i}{\mu_p E_0}p_{\omega_i}(x) = \frac{\alpha\phi_{\omega_i}}{\mu_p E_0}e^{-\alpha x}. \tag{27}$$

The solution is given by

$$n_{\omega_i}(x) = \frac{\alpha\phi_{\omega_i}}{\alpha\mu_n E_0 - i\omega_i}(e^{-\alpha x} - e^{-(i\omega_i/\mu_n E_0)x}), \tag{28}$$

$$p_{\omega_i}(x) = -\frac{\alpha\phi_{\omega_i}}{\alpha\mu_p E_0 + i\omega_i}(e^{-\alpha x} - e^{-\alpha L}e^{(i\omega_i/\mu_p E_0)(x-L)}), \tag{29}$$

which satisfy the boundary condition

$$n_{\omega_i}(0) = 0, \quad p_{\omega_i}(L) = 0. \tag{30}$$

The current density is derived as

$$J_{n,\omega_i}(x) = \frac{q\alpha\mu_n E_0 \phi_{\omega_i}}{\alpha\mu_n E_0 - i\omega_i}(e^{-\alpha x} - e^{-(i\omega_i/\mu_n E_0)x}), \tag{31}$$

$$J_{p,\omega_i}(x) = -\frac{q\alpha\mu_p E_0 \phi_{\omega_i}}{\alpha\mu_p E_0 + i\omega_i}(e^{-\alpha x} - e^{-\alpha L} e^{(i\omega_i/\mu_p E_0)(x-L)}). \tag{32}$$

In the n^+ region, from Eqs. (4) and (7), we derive

$$\frac{d^2 f_{\omega_i}(x)}{dx^2} - \frac{1 - i\omega_i \tau_p}{L_p^2} f_{\omega_i}(x) = -\frac{\alpha}{D_p}\phi_{\omega_i} e^{-\alpha x}, \tag{33}$$

where

$$p(x,t) - p_0 \equiv \sum_{\omega_i} f_{\omega_i}(x) e^{-i\omega_i t}. \tag{34}$$

Imposing the boundary conditions

$$p(L,t) = 0, \quad p(\infty,t) = p_0, \tag{35}$$

we obtain the solution

$$\begin{aligned} p(x,t) - p_0 = \sum_{\omega_i} \Bigg[\Bigg(& - p_0 \delta_{\omega_i 0} \\ & - \frac{\alpha L_p^2}{1 - i\omega_i \tau_p - \alpha^2 L_p^2} \frac{1}{D_p} \phi_{\omega_i} e^{-\alpha L} \Bigg) \\ & \times e^{-\frac{\sqrt{1 - i\omega_i \tau_p}}{L_p}(x-L)} \\ & + \frac{\alpha L_p^2}{1 - i\omega_i \tau_p - \alpha^2 L_p^2} \frac{1}{D_p} \phi_{\omega_i} e^{-\alpha x} \Bigg] e^{-i\omega_i t}. \end{aligned} \tag{36}$$

The current density due to the diffusion is now written as

$$\begin{aligned} J_{\mathrm{diff}}(L,t) &= -qD_p \left(\frac{\partial p(x,t)}{\partial x} \right)_{x=L} \\ &\simeq \sum_{\omega_i} \left[-\frac{q\alpha L_p}{\sqrt{1 - i\omega_i \tau_p} + \alpha L_p} \phi_{\omega_i} e^{-\alpha L} \right] e^{-i\omega_i t}. \end{aligned} \tag{37}$$

Therefore, the total current consisting of the drift and the diffusion components is

$$\begin{aligned} J_{\mathrm{total}}(L,t) &= J_{\mathrm{dr}}(L,t) + J_{\mathrm{diff}}(L,t) = \sum_{\omega_i} J_{\omega_i} e^{-i\omega_i t} \\ &= \sum_{\omega_i} \left[\frac{q\alpha\mu_n E_0}{\alpha\mu_n E_0 - i\omega_i} \left(e^{-\alpha L} - e^{-(i\omega_i/\mu_n E_0)L} \right) \right. \\ &\quad \left. - \frac{q\alpha L_p}{\sqrt{1 - i\omega_i \tau_p} + \alpha L_p} e^{-\alpha L} \right] \phi_{\omega_i} e^{-i\omega_i t}. \end{aligned} \tag{38}$$

If we consider the stationary limit $\omega_i \to 0$, Eq. (38) reduces to Eq. (20). The load resistance R, which is normally connected to photodiode during operation, is not considered in this formulation. As such, it not necessary to take into account displacement current, which is needed to describe the *RC*-constant effect. However, we can easily incorporate such an effect arising from R into our formulation in a similar way as in Ref. 9.

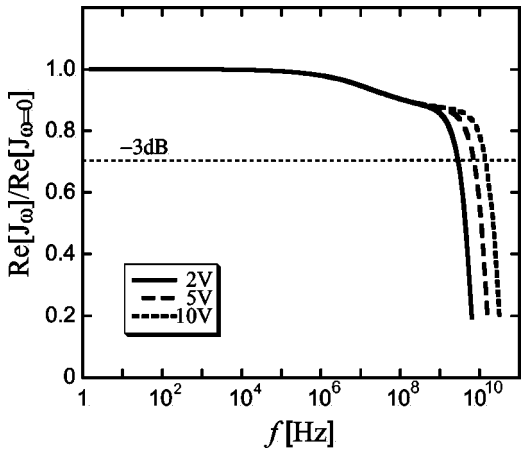

FIG. 3. High frequency response of $L=2$ μm for different applied reverse biases. The response is enhanced at higher applied bias.

B. High frequency characteristics

Using the expression given by Eq. (38) for the current density of each mode, we investigate the high frequency characteristics of the vertical *p-i-n* photodiode. We first discuss the dependence of the high frequency response on applied reverse bias. Figure 3 shows the real part of J_{ω_i} normalized by the value at $\omega_i = 0$ for three applied biases (2V, 5V, and 10 V) for $L=2$ μm. The optical amplitude of each mode is kept equal. (The same results can be derived for any optical intensity in the linear region of optical response.) In these calculations, we have only one device parameter, mobility μ, whose value is adopted as $\sim 500\ \mathrm{cm}^2/\mathrm{V\,s}$. Higher bias slightly improves the response at -3 dB level as expected. The dependence of J_{ω_i} on the length L of the i region is shown in Fig. 4 for a reverse bias of 2 V. We adopted the same value of mobility as given above. The high frequency response falls down for longer L due to longer transit time for carriers. On the other hand, for shorter L, the high frequency response is not necessarily enhanced. As shown in the figure, the response is improved by reducing L to 2 μm.

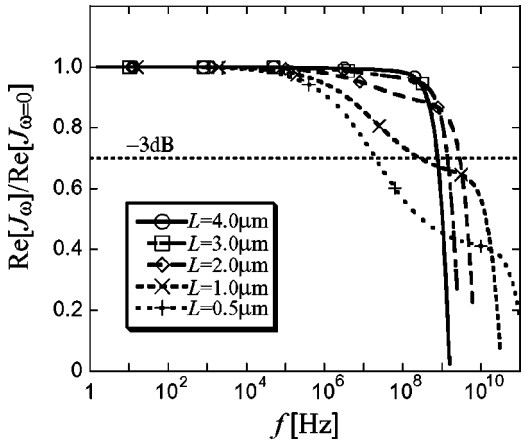

FIG. 4. High frequency response for different i region length L. The cutoff frequency f_T is depicted by the -3 dB line. f_T decreases at short L because of diffusion effects. The reverse bias is 2 V.

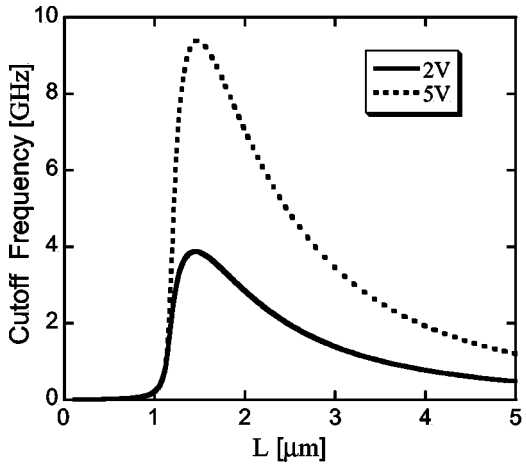

FIG. 5. Cutoff frequency f_T as a function of i region length L. At shorter L, the cutoff frequency is restricted by diffusion effects.

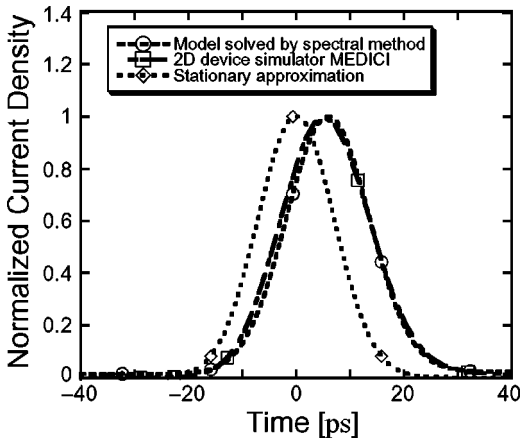

FIG. 6. Accurate calculation of the photocurrent calculated by the model as compared to a two-dimensional device simulator. The stationary approximation is also depicted and a clear delay of the calculated current is observed.

However, beyond this value, the response deteriorates which is attributed to the increasing contribution of the diffusion current. The cutoff frequency f_T (at -3 dB line) as a function of L is shown in Fig. 5. We can see a nonlinear growth of the cutoff frequency at small L, which is different from the linear growth of RC-constant effect (see also Ref. 9). Therefore, there is an optimum length of the i region to obtain a high frequency response as shown in Fig. 1. When R is present, the linear effect of the RC constant restricts the visibility of the diffusion current effect depending on the value of R. In the limiting case where $R \to 0$, diffusion alone decides the cutoff frequency at short L.

C. Simulation results based on the spectral method

In order to show the validity of the solution obtained in Eq. (38), we simulate the full nonstationary response of the photodiodes. For this purpose, we adopt the spectral method, which is composed of the following procedure.

(1) Expanding input optical signals into Fourier modes with single frequency ω_i by using Fast Fourier Transform.[13]
(2) Deriving the solution of output current for each mode labeled by ω_i.
(3) Summing up the Fourier modes of current to construct the final output current in real space.

The second step is already discussed in the preceding section.

Using the above-mentioned numerical method, we calculated the photocurrent for a Gaussian light pulse of intensity $I(t)=I_0 \exp(-t^2/\sigma^2)$, whose normalized values are shown in Fig. 6. Here we adopted $\sigma=10$ ps. (The weak intensity of the light pulse validates the assumption that the electric field induced by the applied voltage is not affected by the incident light.) We considered a Si vertical p-i-n photodiode with $n^+ \sim 10^{20}$ cm^{-3}, $p^+ \sim 10^{20}$ cm^{-3}, and $n(i$ region$) \sim 10^{15}$ cm^{-3}. The incident light wavelength λ is 532 nm, where the corresponding optical absorption coefficient α is ~ 1 μm^{-1}. We also compared the result with that obtained by the stationary approximation and that obtained by a commercial two-dimensional numerical device simulator MEDICI.[14] Only the mobility parameter is changed ($\mu \simeq 550$ cm^2/V $\cdot$s) in order to reproduce the MEDICI result. This is justified by the fact that for any device model, parameter extraction is usually applied before performing circuit simulation. Calculation results with our proposed model can reproduce the nonstationary feature obtained by the MEDICI simulation. The nonstationary feature is delayed as shown in Fig. 6.

V. SUMMARY

We have obtained the analytical current density description for p-i-n photodiodes in Fourier space and investigated the high frequency photoresponse using our description. For shorter i region length, we have shown that diffusion restricts the cutoff frequency in the limit of zero load resistance R. We also developed a simulation scheme based on the spectral method. With a significant reduction in computation time, the current characteristics calculated by our model are comparable to two-dimensional device simulation results.

Our formulation developed in this paper is very easy to use and compatible to the harmonic balance simulation of circuits,[15] which is a powerful method for analyzing high frequency and/or nonlinear circuits. Therefore, our result is very useful to perform such simulation of OEICs.

[1] M. Dentan and B. de Cremoux, J. Lightwave Technol. **8**, 1137 (1990).
[2] J. B. Radunović and D. M. Gvozdić, IEEE Trans. Electron Devices **40**, 1238 (1993).
[3] Y. Leblebici, M. S. Ünlü, S.-M. Kang, and B. M. Onat, J. Lightwave Technol. **13**, 396 (1995).
[4] P. S. Matavulj, D. M. Gvozdić, and J. B. Radunović, J. Lightwave Technol. **15**, 2270 (1997).
[5] G. Lucovsky, R. F. Schwarz, and R. B. Emmons, J. Appl. Phys. **35**, 622 (1964).
[6] J. E. Bowers, C. A. Burrus, and R. J. McCoy, Electron. Lett. **21**, 812 (1985).
[7] J. E. Bowers, and C. A. Burrus, J. Lightwave Technol. **LT–5**, 1339 (1987).
[8] R. Sabella, and S. Merli, IEEE J. Quantum Electron. **29**, 906 (1993).
[9] G. Torrese, A. Salamone, I. Huynen, and A. Vander Vorst, Microwave Opt. Technol. Lett. **31**, 329 (2001).
[10] See, e.g., B. Mercier, *An Introduction to the Numerical Analysis of Spectral Methods* (Springer, Berlin, 1989); C. Canuto, M. Y. Hussaini, A. Quarteroni, and T. A. Zang, *Spectral Methods in Fluid Dynamics* (Springer, Berlin, 1988).

[11]O. Matsushima, K. Konno, M. Tanaka, K. Hara, and M. Miura-Mattaush, Semicond. Sci. Technol. **19**, S185 (2004); K. Konno, O. Matsushima, D. Navarro, and M. Miura-Mattausch, Appl. Phys. Lett. **84**, 1398 (2004).
[12]S. M. Sze, *Physics of Semiconductor Devices* (Wiley, New York, 1981).
[13]W. H. Press, S. A. Teukolsky, W. T. Vetterling, and B. P. Flannery, *Numerical Recipes in Fortran 77* (Cambridge University Press, Cambridge, 1992).
[14]*MEDICI User's Manual*, Synopsys (2002).
[15]See, e.g., K. S. Kundert and A. Sangiovanni-Vincentelli, IEEE Trans. Comput.-Aided Des. **CAD-5**, 521 (1986).